PERGAMON

Journal of Structural Geology 22 (2000) 1027–1047

JOURNAL OF STRUCTURAL GEOLOGY

www.elsevier.nl/locate/jstrugeo

The geometry, kinematics and rates of deformation within an en échelon normal fault segment boundary, central Italy

Nigel C. Morewood*, Gerald P. Roberts

The Research School of Geological and Geophysical Sciences, Birkbeck and University College London, Gower Street, London WC1E 6BT, UK

Received 21 July 1999; accepted 22 March 2000

Abstract

The geometry, kinematics and rates of deformation have been investigated within an en échelon fault segment boundary between two left-stepping major normal faults in the central Apennines, Italy. Examination of faulted post-glacial sediments and geomorphic features attributed to glacial retreat (18 ka) reveals that the two major faults dominate the recent slip, with rates that are 5–10 times greater than the other faults. At the centres of the major faults, slip is parallel to the regional extension direction (NE–SW) defined by focal mechanisms and borehole breakouts. Slip-vector azimuths defined by striations on faults in the stepover zone indicate NE–SW extension on NW–SE faults, sub-parallel to the regional extension direction, together with significant and contemporaneous NW–SE extension, along the strike of the Apennines, on ESE–WNW and ENE–WSW faults. Thus, distributed three-dimensional strain occurs in the stepover between the two major bounding faults. Extension rates summed across the stepover are 0.68 mm/y parallel to the regional extension, compared to ~2 mm/y at the centre of one of the major faults. Extension rates along-strike of the fault zone are 0.14 mm/y within the stepover and zero at the centres of the two major bounding faults. The above information is used to discuss how extension is partitioned between different structures during the growth and linkage of normal faults.

1. Introduction

It is generally accepted that long, basin-bounding normal fault zones develop through linkage of shorter faults. Some of these faults occur along-strike of each other but also commonly form en échelon geometries. Many studies have recognised these stepovers as areas of displacement transfer and eventual fault linkage (Peacock and Sanderson, 1991, 1994; Anders and Schlische, 1994; Trudgill and Cartwright, 1994; Dawers and Anders, 1995; Cartwright et al., 1995, 1996; Cowie, 1998). However, we are not aware of any studies that document the geometry, kinematics and rates of deformation in stepovers prior to linkage. The lack of information on the rates of deformation means that it is unclear how the finite structures develop and thus how deformation proceeds from a stepover geometry to a zone of fault linkage.

In this paper we describe the geometry, kinematics and rates of deformation within the Velino fault segment boundary (VFSB), an area which lies in the stepover between two en échelon faults in the central Apennines, Italy. The VFSB is an important structure concerning seismic hazard in the region, as it marks the northwestern extent of the surface rupturing produced during the 1915 Fucino earthquake [$M_s = 7.0$; ~33,000 fatalities (Margottini and Screpanti, 1988)]. Through examination of faulted post-glacial sediments and slopes formed by glacial retreat, we show that the two large faults forming the stepover have higher slip-rates than those within it. Moreover, these major en échelon faults appear to control the slip directions on the minor faults within the stepover, producing significant along-strike extension. We use our findings to discuss how extension is partitioned between different

* Corresponding author.
E-mail address: n.morewood@ucl.ac.uk (N.C. Morewood).

0191-8141/00/$ - see front matter
PII: S0191-8141(00)00030-4

(a)

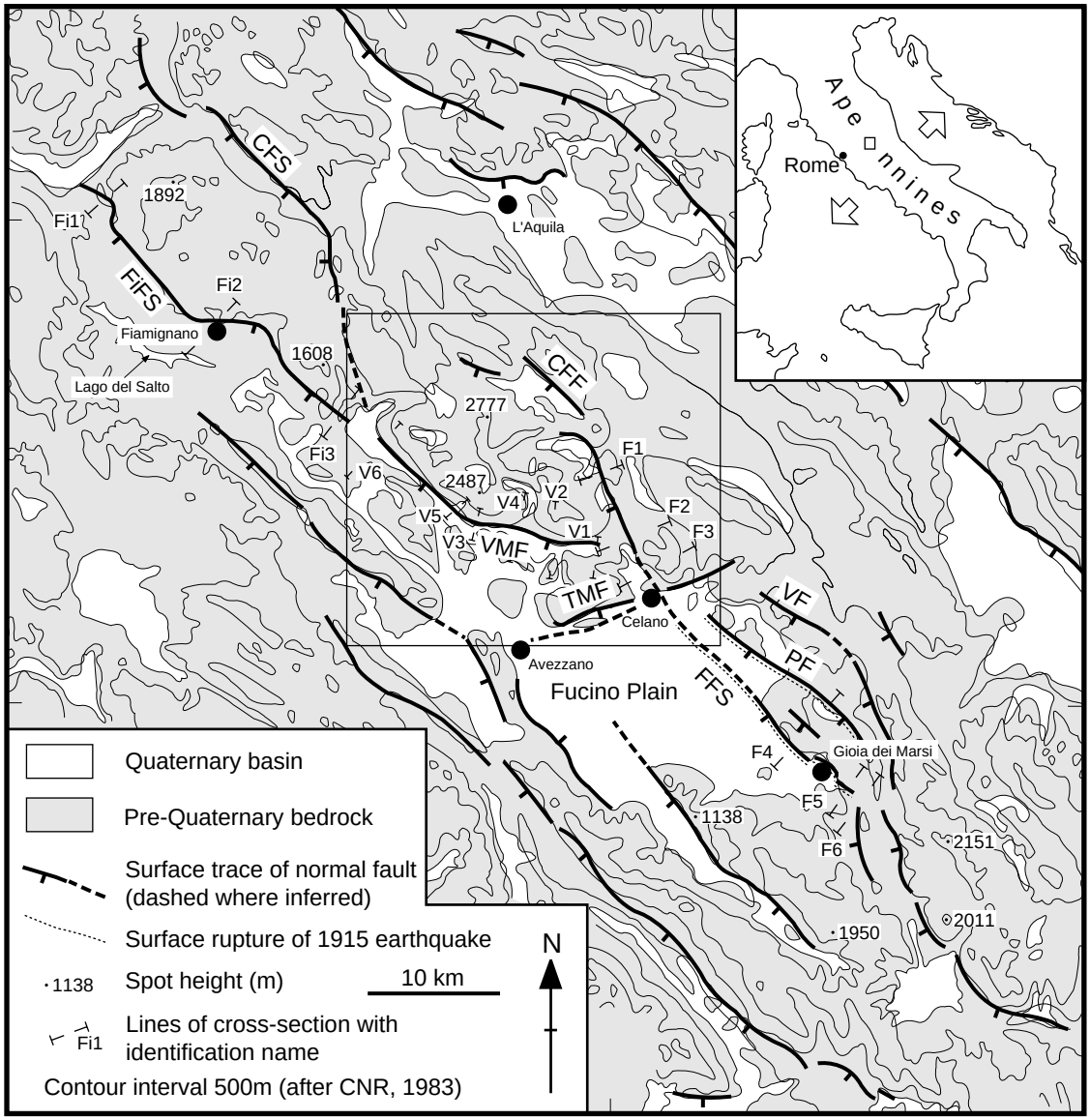

Fig. 1. (a) Map of the Abruzzo region, located by the box in the inset, showing the relationship between the major normal faults and the Quaternary basins in their hanging walls. Some faults do not have thick hanging wall basin fill because it has been removed by river incision (e.g. FiFS). The faults referred to in the text are labelled as follows: FiFS—Fiamignano fault segment; FFS—Fucino fault segment; CFF—Campofelice fault; VMF—Velino–Magnola fault; TMF—Tre Monti fault; CFS—Corno fault segment; PF—Parasano fault; VF—Ventrino fault. The box locates Figs. 5(a) and 9. (b) Map of studied faults with fault-trace thickness proportional to the rate of horizontal extension since 18 ka in the plane of slip at each locality. The back (NE) edge of each fault represents the map trace shown in Fig. 1(a). The FiFS and FFS have been the most active faults over this period and form an en échelon step in the fault system. The faults within the stepover or segment boundary (VFSB) are smaller and less active than the major faults. The stereonets (lower hemisphere) show poles to fault planes (open squares) and lineations (striations, corrugations) on the fault planes (filled circles). Arrows indicate the mean fault-slip direction for each locality. Locality details are in Tables 1 and 2. 'X' indicates the centre of the FFS used for measurement purposes in producing Fig. 9(b). See text for discussion.

structures during the development of stepovers and following linkage.

2. Tectonic setting

The Velino–Fucino area lies within the Apennine mountain chain (Fig. 1a), a NW–SE-trending structure that formed in the convergent zone between the African and Eurasian plates. In the central Apennines shortening persisted until the middle to late Pliocene (Patacca et al., 1990). Present day extension occurs across active normal faults striking generally parallel to the mountain chain (Anderson and Jackson, 1987). The central and southern Apennines comprise an 800-km-long system of seismogenic segmented normal

(b)

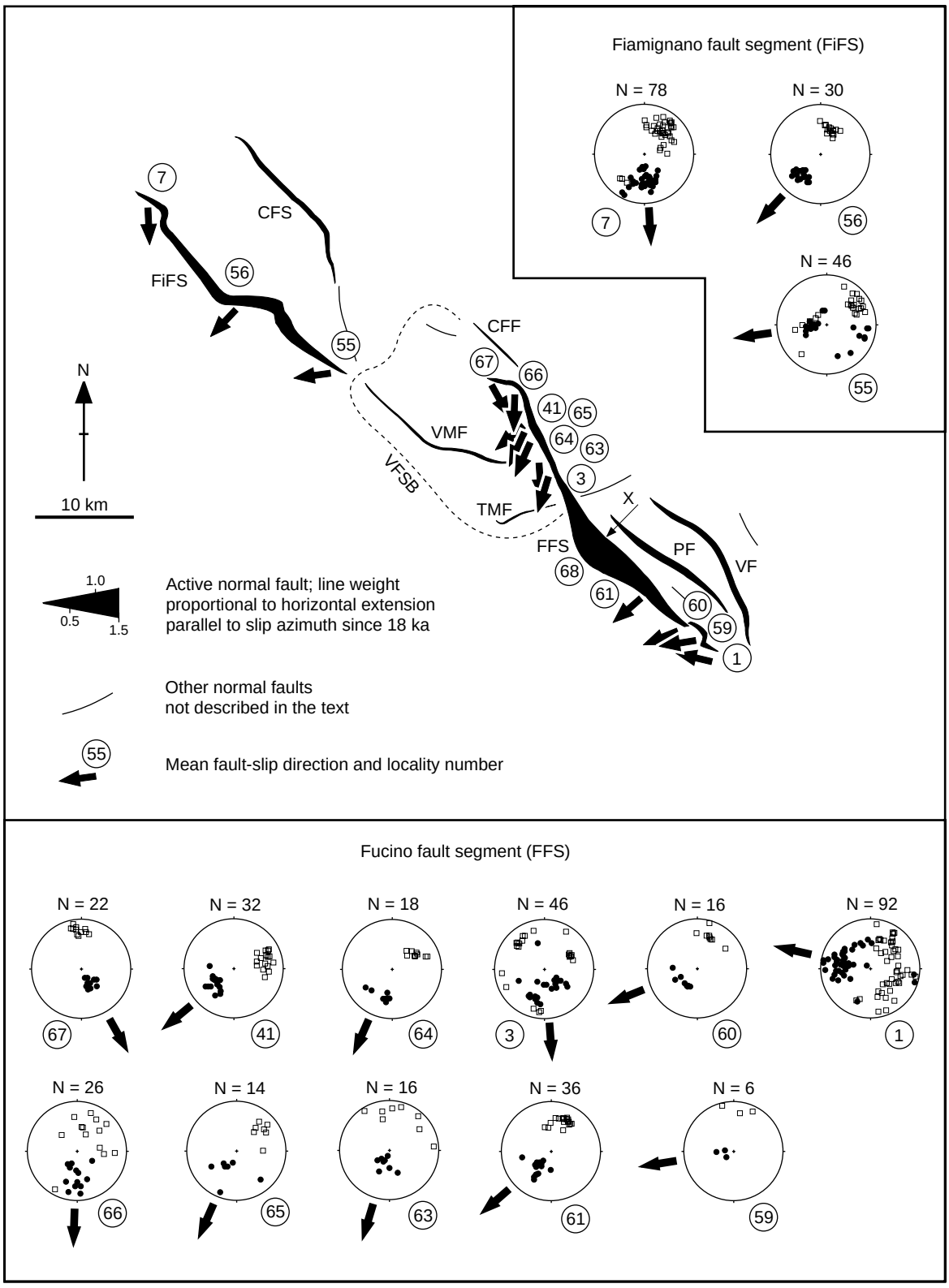

Fig. 1 (*continued*)

faults that accommodates most of the present NE–SW (~225°) extension, determined from earthquake focal mechanisms, fault-slip and borehole breakout data (Anderson and Jackson, 1987; Ward and Valensise, 1989; Westaway et al., 1989; Amato et al., 1995; Amoruso et al., 1998).

In this paper we are concerned with the area close to the ruptures produced by the 1915 Fucino earthquake. The 30–90 cm of surface slip produced by this earthquake occurred along the normal fault bounding the NE side of the Fucino basin (Fig. 1a) (Oddone, 1915; Serva et al., 1988; Margottini and Screpanti, 1988; Ward and Valensise, 1989; Blumetti et al., 1987). Below we study the map traces, throws, slip directions and throw rates associated with this and other normal faults in the region (Figs. 1–8). We have found that two faults dominate the recent slip, with rates about 5–10 times greater than the other normal faults. One of these is the fault that ruptured in 1915; the other is a fault further to the northwest. These two faults form a left-stepping en-échelon geometry. Other faults exist in the stepover zone. Below we describe our methodology and the geometry, kinematics and rates of deformation along the faults in the region before discussing the implications of the study.

3. Methodology

The Velino–Fucino area provides an exceptional opportunity to study the geometry, kinematics and rates of deformation within a stepover because it contains well-exposed striated faults that offset Mesozoic bedrock, and sediments and geomorphic surfaces associated with the last major glacial phase that occurred in the region (ca. 18 ka; Giraudi and Frezzotti, 1997). We have mapped the positions of faults, measured fault plane and lineation orientation data and determined throw at a number of localities within the study area. We have also deduced rates of deformation from displaced post-glacial sediments and geomorphic features associated with glacial retreat. We combine and compare our data with published rates from offset Holocene soils investigated during palaeoseismic trenching studies conducted within the study area. Overall, these data constrain the geometry, kinematics and rates of deformation associated with the faults in the Velino–Fucino area.

The surface traces of faults in the study area have been determined by checking (in the field) of published data and new mapping (Figs. 1, 5a, 6–8). The positions of studied localities were located using 1:100,000 topographic maps and a hand-held GPS receiver and are accurate to ±50 m with respect to each other. In order to calculate the total throw across the faults a series of cross-sections were constructed across the faults using published geological maps (Fig. 2a). The accuracy in measuring the total throw is constrained by the resolution of the available maps and errors are usually less than about ±200 m. Lineation data (striations, corrugations) were collected at most of the studied localities. Measurements were made of all lineations that intersected horizontal transects across fault plane outcrops. The mean slip direction was calculated for each locality using Bingham statistics.

At many localities the faults offset late Pleistocene fluvioglacial fan surfaces or slopes that achieved their final form during the last glaciation and, more rarely, moraines associated with glacial retreat. The end of outwash sedimentation related to the retreat phases of the Majelama Valley (Mt. Velino; Fig. 5a) glacier occurred prior to ca. 16 ka (Giraudi and Frezzotti, 1997). This coincides with a major glacier retreat phase in the central Apennines, which began at 17.84 ± 0.2 ka, ended at ca. 16 ka and dominates the geomorphology of the region (Giraudi and Frezzotti, 1997). This rapid phase of glacier retreat marks a major climatic change in the Mediterranean area and corresponds to an abrupt decrease in the $\delta^{18}O$ values recorded in Tyrrhenian Sea cores (Giraudi and Frezzotti, 1997). Other, minor glacial phases occurred at about 15, 14 and 13 ka, but they did not have a marked effect on the geomorphology of the study area (Giraudi and Frezzotti, 1997). Away from the faults, smooth, uniform periglacial slopes and fluvioglacial fans exist, commonly covered with a thin layer (1–2 m) of post-glacial organic-rich soil. These define surfaces dating from about the same time as the major glacial retreat stage (18–16 ka; see Giraudi and Frezzotti, 1997). Recent palaeoseismic studies report slip-rates for faults that offset these and younger, dated (usually ^{14}C) soil horizons (e.g. Pantosti et al., 1996). Where such dates are unavailable, slip-rates can be estimated by assuming an age for the offset late-/post-glacial surface. Unless data are available to the contrary, we assume an age of 18 ka for the late-/post-glacial surfaces, which yields minimum slip-rates. If a surface does actually date from 16 ka, our method produces negligible error in slip-rates for a roughly 1-m-high scarp and underestimates the slip-rate on 10-m- and 30-m-high scarps by 0.07 and 0.21 mm/y, respectively.

In order to measure the throw that has accumulated since ca. 18 ka, topographic profiles were constructed at each locality in order to gain the true vertical offset of the glacial surfaces. Because of the dip of the glacial surfaces and erosion of the fault scarps, the amount of vertical offset can be overestimated by measuring the height of the exposed fault scarp only (Fig. 2b). We believe that the errors associated with throw measurement from the scarp profiles are negligible for scarps up to 10 m high and no greater than ±2.0 m for scarps

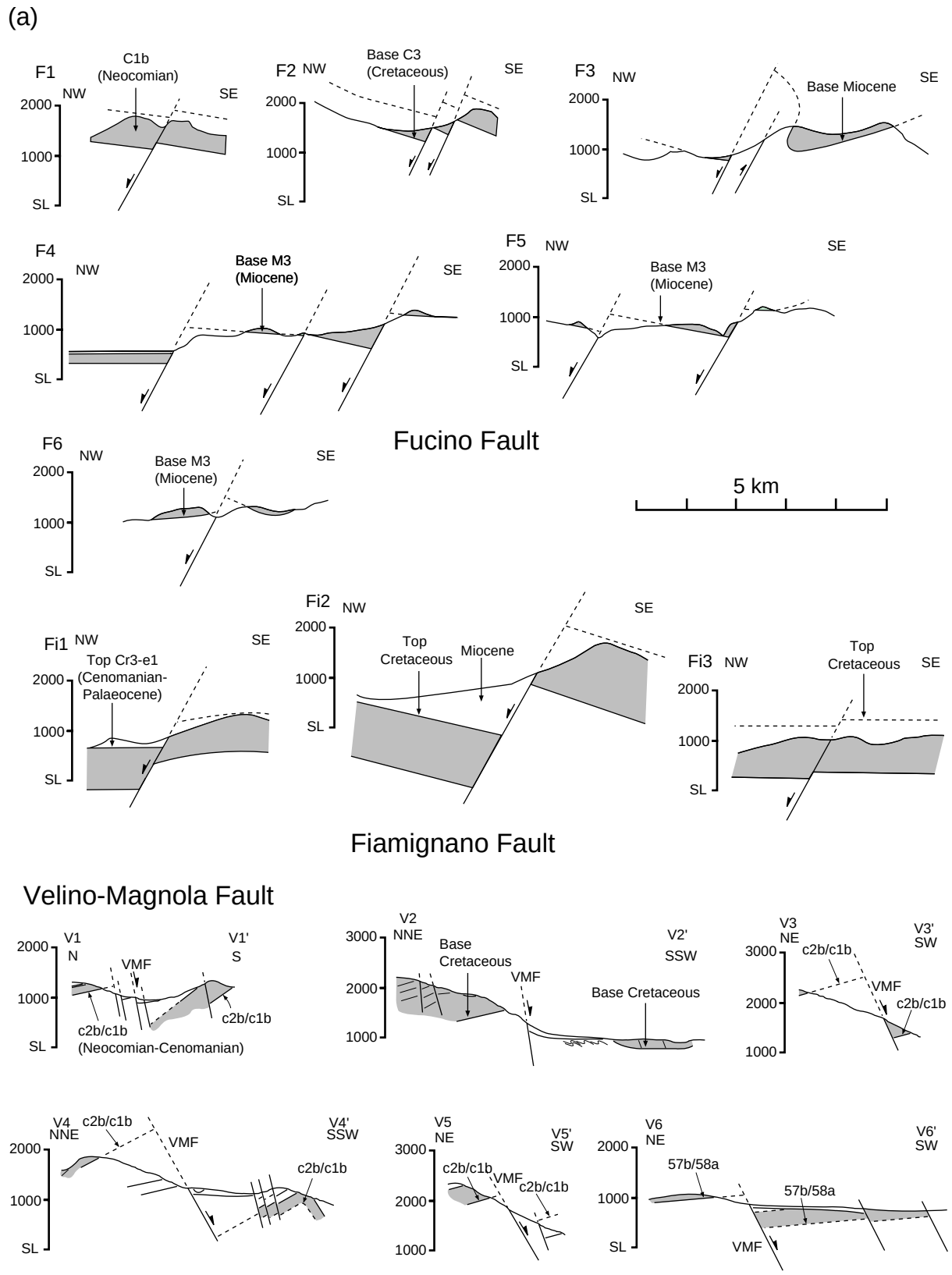

Fig. 2. (a) Cross-sections (located in Fig. 1a) through the Fiamignano, Fucino and Velino–Magnola faults. In each section a marker horizon (labelled) was used to measure the throw and the unit above or below this horizon is shaded for clarity. The geological markers are taken from Nijman (1971) with the exceptions of sections Fi1, Fi2, Fi3 and V6, which are from C.N.R. (1983). No vertical exaggeration. (b) Representative topographic profiles across the Fucino (FFS), Tre Monti (TMF) and Velino–Magnola (VMF) faults. The vertical separation of geomorphic features (shaded) offset by the scarps since 18 ka is given in metres (see text for details). Profile locations are given in Figs. 5(a), 6 and 8.

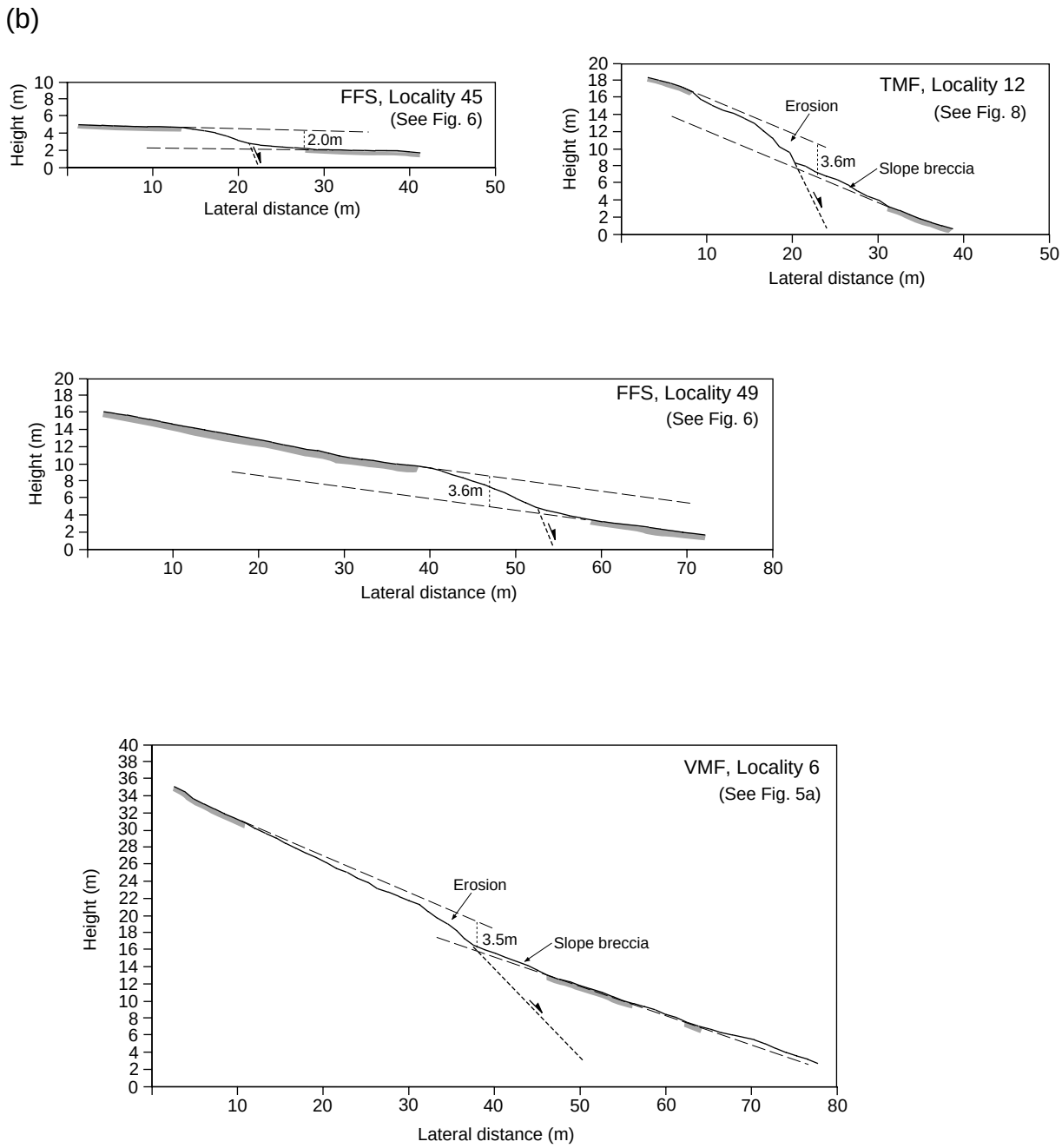

Fig. 2 (*continued*)

10–25 m high and ±5.0 m for scarps 25–40 m high. These errors, combined with those involved in estimating the age of the offset glacial surfaces (18–16 ka) give errors in throw rate of about +0.11/−0.18 and +0.28/−0.49 mm/y for scarps 10 m and 30 m high, respectively. All errors are shown by bars on the appropriate graphs. Because we use an age of 18 ka for the late-/postglacial surfaces in order to minimise the slip-rates (see above), the error in estimating the timing of the last glacial phase becomes almost irrelevant when considering the relative rates of slip across the faults. The combined errors shown on the graphs may therefore be viewed as maximum errors for the data.

Minimum estimates of throw rate averaged over the past 18 ka were attained by dividing the vertical offset by 18,000 years. By combining throw rates derived in this manner with other values from trenches and with the fault-slip data described above we have calculated rates of throw, displacement and horizontal extension for the vertical plane containing the mean slip direc-

tion at each locality (Tables 1 and 2). Where no fault-slip data is available, displacement and horizontal extension have been calculated using a fault dip of 70° for the NW part of the Fucino fault (FFS) and 65° for the Tre Monti fault (TMF) and by using the slip direction of the nearest locality with data (see Tables 1 and 2).

4. Results

In order to investigate fault segmentation within the study area we plotted total throw against distance along-strike for the faults (Fig. 3a). This has distinguished three large faults, each with a maximum throw in the centre, tapering to a minimum at each end (FiFS, FFS, VMF) and a number of shorter faults with smaller throws (Fig. 1b). A plot of throw since ca. 18 ka as a function of distance shows a similar pattern for the three large faults (Fig. 3b). Thus, the pattern of throw distribution over the period 18–0 ka appears to have been similar to the averaged total throw distribution.

We have also plotted throw rate over the past 18 ka (from displaced geomorphic features and trench data, as discussed above) against total throw (measured from geological cross-sections) for each of the FFS, FiFS and VMF (Fig. 4a–c). This shows a good linear correlation between recent throw and total throw for the FFS, FiFS and VMF: the values of highest recent (18–0 ka) and total throw occur at the same place, as do the values of lowest recent throw and lowest total throw. This increases confidence in our throw and throw-rate measurements. Fig. 4(d–f) shows recent throw rate plotted as a function of distance (normalised to a 100 km long fault) from the centres of the FFS, FiFS and VMF. For each fault, the throw rate since 18 ka is highest at the fault centre and decreases to minima towards the ends (Fig. 4d–f). These plots allow direct comparisons of the spatial and temporal throw distributions associated with the different faults to be made. Below we discuss each fault in more detail.

4.1. The Fucino fault segment (FFS)

The FFS is a NW–SE- to N–S-trending normal fault which downthrows to the SW (Fig. 1). Fig. 3(a) shows that the FFS has a maximum total throw of about 2200 m, which decreases to 300–400 m at approximately the same distance (~20 km) to the NW and SE of the point of maximum throw. On the basis of our throw profiles the FFS is at least 40 km in length. The northwestern part of the FFS bounds the northeastern border of the stepover between it and the FiFS (Fig. 1). The maximum throw occurs where the fault is poorly exposed as it crosses Quaternary lake sediments of the Fucino basin (Locality 68, Fig. 1b). The maximum throw is estimated by summing throws across the Fucino fault at Locality 61 (Figs. 1b and 2a) and the Parasano (600 m) and Ventrino (>600 m) faults and an estimated thickness (>400 m) of Quaternary sediments in the hanging wall of the FFS in the Fucino basin. This value (2200 m) produces a realistic throw/distance profile with the maximum throw near the centre of the fault (Fig. 3a).

The FFS outcrops as a limestone fault scarp for about 8 km along the northern slopes of Piano di Pezza to the western slopes of Mt. delle Canelle (Fig. 6) (see also Biasini, 1966; Giraudi, 1989; Cinti et al., 1992; Pantosti et al., 1996). South of the Park Hotel (Fig. 6), Mesozoic limestone slip surfaces outcrop in places as far as the town of Celano (Fig. 5a). The FFS continues southeast, crossing the Fucino plain and then in places bounding the Fucino basin, as far as a few kilometres southeast of the village of Gioia dei Marsi (Fig. 1).

The northwestern end of the FFS has two main splays, north and south of the Valle dell Ortica (Fig. 6). Limestone scarps of the northern splay strike 090–110° and dip 50–80°. No slip surfaces crop out on the southern splay but the scarp, offsetting Wurm III moraines, strikes on average 090° and downsteps to the west. The scarp changes strike to ~130° as it crosses the Piano di Pezza, west of Vado di Pezza and reverts to 110° (Locality 47, Fig. 6) before striking N–S through Mt. delle Canelle, West of Mt. delle Canelle a 2 km splay, striking 120–170°, bounds the northeastern edge of Campo di Via (Fig. 6). South of Mt. delle Canelle a sub-parallel antithetic fault forms a small graben (see Pantosti et al., 1996).

The mean slip direction of all localities for the FFS is towards 223° (Table 1), very close to the regional extension direction of 225°. The FFS exhibits a converging pattern of slip vectors with dip-slip motion across the central portion of the fault and oblique-slip at its lateral tips (Fig. 1b). This is a similar pattern of slip to that described by for normal faults in central Greece (Roberts, 1996; Roberts and Ganas, 2000) and in southern Italy (Michetti et al., 2000).

Scarp height (offsetting the 18 ka surface) varies from 0.5 m at the northwestern end of the FFS (Locality 18) to 2.0 m at Locality 46 (Fig. 6), 1 km further east. South of Mt. delle Canelle the fault scarp is up to 12 m in height and bounds the eastern edge of an active alluvial fan (Locality 41, Fig. 6; Table 1). Pantosti et al. (1996) observed a 12 m offset of late Pleistocene and Holocene fluvioglacial fan and moraine deposits ~300 m south of our Locality 41. Slip directions vary from 130 to 236° along the main scarp, with a mean slip direction for all localities towards 174° (Fig. 6; Table 1), about 50° different to the 225° re-

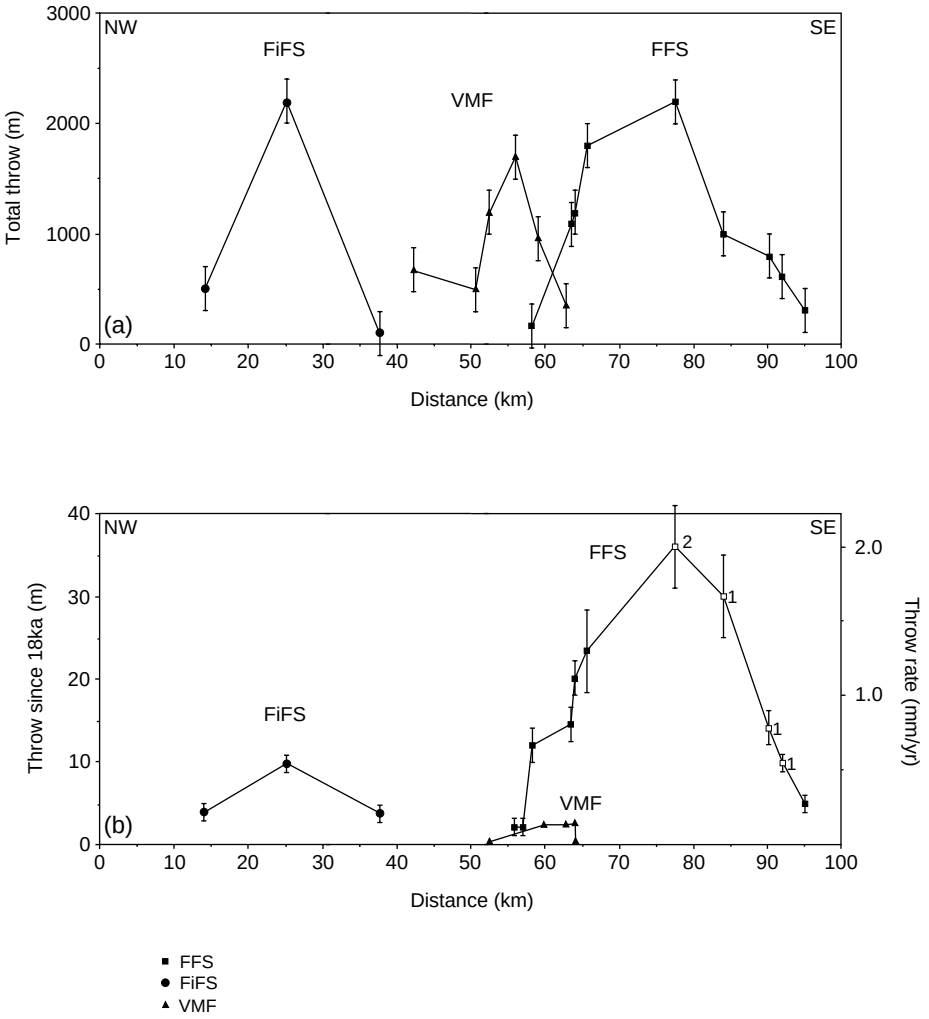

Fig. 3. (a) Total throw vs. distance profile for the studied fault system. (b) Throw since 18 ka as a function of distance along the same fault system. Closed symbols: offset postglacial sediments and other observations described in this study; open symbols: published trench data from (1) Galadini et al. (1997) and (2) Michetti et al. (1996). FiFS—Fiamignano fault segment; VMF—Velino–Magnola fault; FFS—Fucino fault segment. See text for discussion.

gional extension direction derived from focal mechanisms (Anderson and Jackson, 1987; Ward and Valensise, 1989; Westaway et al., 1989).

The FFS offsets Holocene and modern fan surfaces and late Pleistocene (ca. 18 ka) fluvioglacial deposits and moraines (Fig. 6). Using this information, published trench data and the rationale outlined above, minimum deformation rates for the faults which offset these deposits can be calculated (Table 1). Rates of throw and displacement range from 0.02–2.00 mm/y and 0.02–2.13 mm/y, respectively. Rates of horizontal extension across the FFS range between 0.01 and 1.60 mm/y (Fig. 1b; Table 1).

Our results are consistent with the findings of Pantosti et al. (1996) who estimated a vertical slip rate across the northwestern part of the FFS (their Ovindoli–Pezza fault) of 0.6–1.1 mm/y (through trenching) and 0.8–2.3 mm/y (through offset geomorphic features), with the lower part of these intervals preferred. These authors showed that the rates obtained from offset geomorphic features and from trenching are comparable when considering the northwestern part of the FFS. Their trench site A in the Piano di Pezza (Fig. 6) yielded a Holocene vertical slip rate of 0.60 mm/y. This is reasonably comparable with our longer term (18 ka) rate of 0.22 mm/y at Locality 49, about 150 m west of their site A (Fig. 6; Table 1). Near the Park Hotel (Fig. 6), Pantosti et al. (1996) used an offset fluvioglacial fan to estimate vertical slip rates of 0.64 mm/y (their Profile I, fig. 4; Fig. 6) and 0.61 mm/y (their Profile II, fig. 4; Fig. 6). This compares favourably with our rate of 0.61 mm/y for an offset fan, about 500 to the north (Locality 41, Fig. 6). The close agreement of our rates, using offset geomorphic fea-

tures, with those from trenching and other studies lends confidence to the techniques and also to the rates derived below for other faults in the area.

4.2. The Fiamignano fault segment (FiFS)

The FiFS is a NW–SE-trending normal fault that downthrows to the SW (Fig. 1). The FiFS has a maximum throw of at least 2200 m, decreasing to 100–500 m to the NW and SE (Fig. 3a). A scarp is traceable at the surface for about 12 km NW and SE of the town of Fiamignano (Fig. 1). The throw/distance profile (Fig. 3a) shows the FiFS has a length of at least 24 km.

The central portion of the FiFS has a mean slip direction of 223° (Table 1), very close to the regional extension direction of 225°. The FiFS shows a similar pattern of slip vectors to the FFS with slip sub-parallel to the regional at the centre of the fault and oblique-slip, converging towards the hanging wall at its ends. Scarp height (offsetting 18 ka sediments) varies from 10 m in the centre of the fault to 4 m and less towards its lateral tips (Table 1). Rates of throw and displacement range from 0.22–0.56 mm/y and 0.32–0.84 mm/y, respectively. Rates of horizontal extension across the FiFS range between 0.23 and 0.64 mm/y (Fig. 1b; Table 1).

4.3. The Velino–Magnola fault (VMF)

The Velino–Magnola fault outcrops in Upper Cretaceous–Palaeocene limestone along the southern slopes of Mt. Magnola and Mt. Velino (Fig. 5a). The fault probably continues as far west as the village of S. Stefano, but is poorly defined as it crosses il Cammerone (Locality 33, Fig. 5a). The fault trends NW–SE from S. Stefano to the slopes of Mt. Velino and then strikes E–W to ESE–WNW towards the village of S. Iona (Fig. 5a). In places the main fault appears to be cut by small N–S-trending cross-faults, which exhibit dip-slip kinematics, but there is no clear temporal relationship. Lower to middle Pleistocene continental sediments are exposed in the hanging wall of the main fault, which also offsets glacial surfaces. Scarp height has not been determined towards the ends of the fault, probably because of their small size, but reaches 5.0 m in the central portion of the fault (Locality 32, Fig. 5a and Table 2). Fault striae indicate mostly

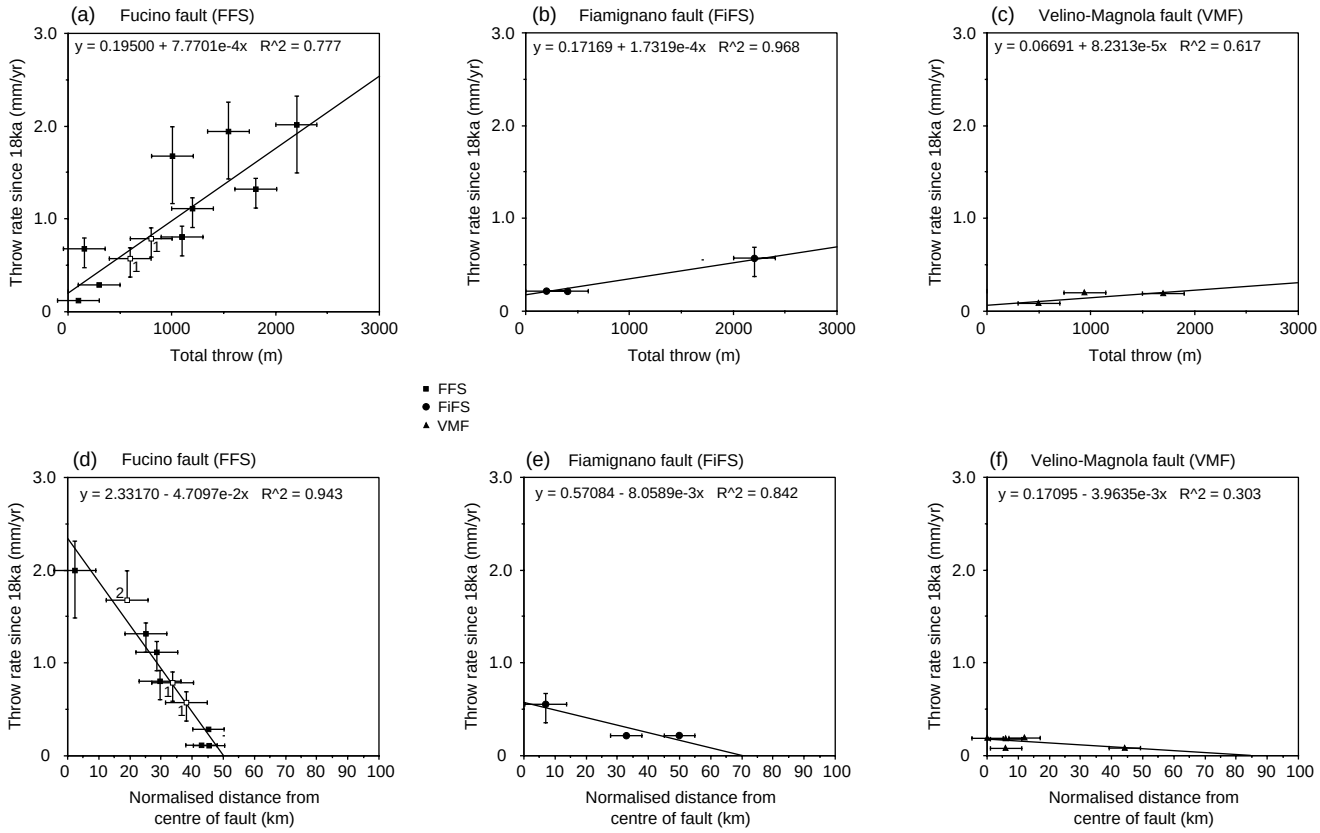

Fig. 4. Throw rate since 18 ka plotted as a function of total throw (a–c) and normalised distance from the centres of the faults (d–f) for the Fucino (FFS), Fiamignano (FiFS) and Velino–Magnola faults (VMF). Symbols as Fig. 3. Errors (indicated by bars) vary with scarp height and are discussed in the text. In (d) the throw rate data from Michetti et al. (1996) are given as a minimum only, as assigned by these authors.

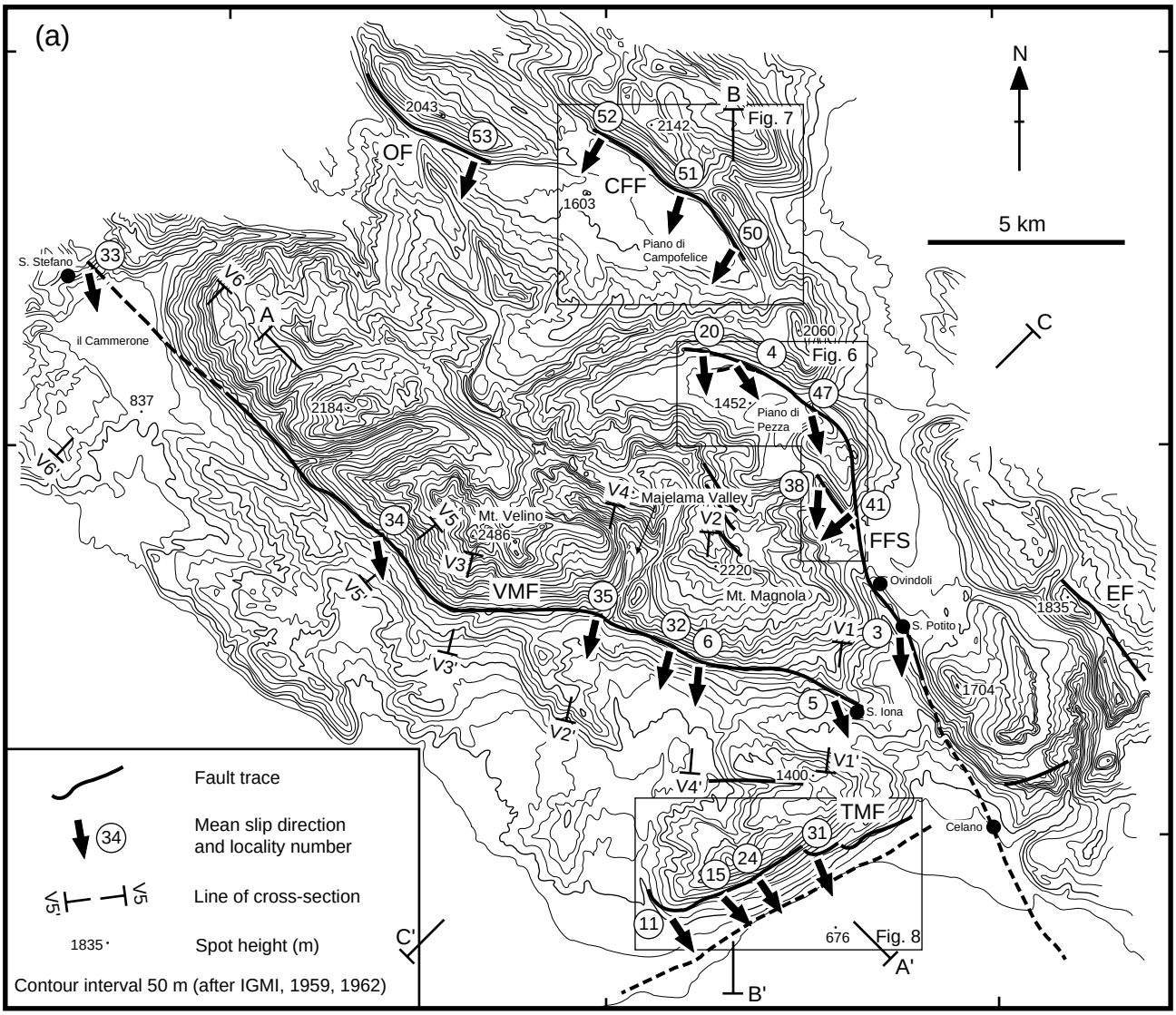

Fig. 5. (a) Map of the Velino fault segment boundary (VFSB), showing the positions of the major normal faults. Heavy arrows show mean fault-slip directions for selected localities along the faults (see Tables 1 and 2). Other slip data are shown in Figs. 6–8. Lines A–A′, etc., indicate positions of cross-sections shown in (b). Lines V1–V1, etc., indicate the positions of cross-sections across the Velino–Magnola fault (VMF) shown in Fig. 2. OF—Orsello fault; CFF—Campofelice fault; FFS—Fucino fault; TMF—Tre Monti fault; EF—Etra fault. (b) Cross-sections, located in (a), showing the structure of the VFSB. Bedding dip is shown by lines where data allow. No vertical exaggeration.

dip-slip movement, at least at the eastern end, across the VMF. Slip directions vary from 159–194° along the main scarp, with a mean slip direction towards 182° (Table 2), over 40° different to the regional extension direction. The VMF does not exhibit the converging slip pattern described for the FFS and FiFS (Fig. 5a).

The VMF displaces glacial till and geomorphic surfaces (Giraudi, 1992, 1995). As discussed above, we assume an age of 18 ka for these features and attain minimum rates of deformation across the fault. This yields rates of throw and displacement of 0.08–0.19 mm/y and 0.09–0.23 mm/y, respectively, and rates of horizontal extension of 0.04–0.17 mm/y (Table 2).

The VMF has a maximum throw of 1700 m, decreasing to 350–500 m, and a length of at least 21 km (Figs. 3a and 5a). Although these are characteristics similar to the FiFS and FFS, the VMF differs from the FiFS and FFS in three main ways: (1) the VMF has a different strike (083–124°) to the FiFS and FFS (mean strike 128° and 134°, respectively) (Fig. 1; Tables 1 and 2); (2) slip on the VMF is directed to the south (mean slip direction 182°) (Fig. 5a; Table 2) as opposed to the FiFS (221°) and FFS (218°), which have mean slip-vectors sub-parallel to the regional extension direction (Fig. 1b; Table 1); (3) the VMF has a low throw rate over the past 18 ka (a third of the throw on the FiFS and only a tenth of that on the

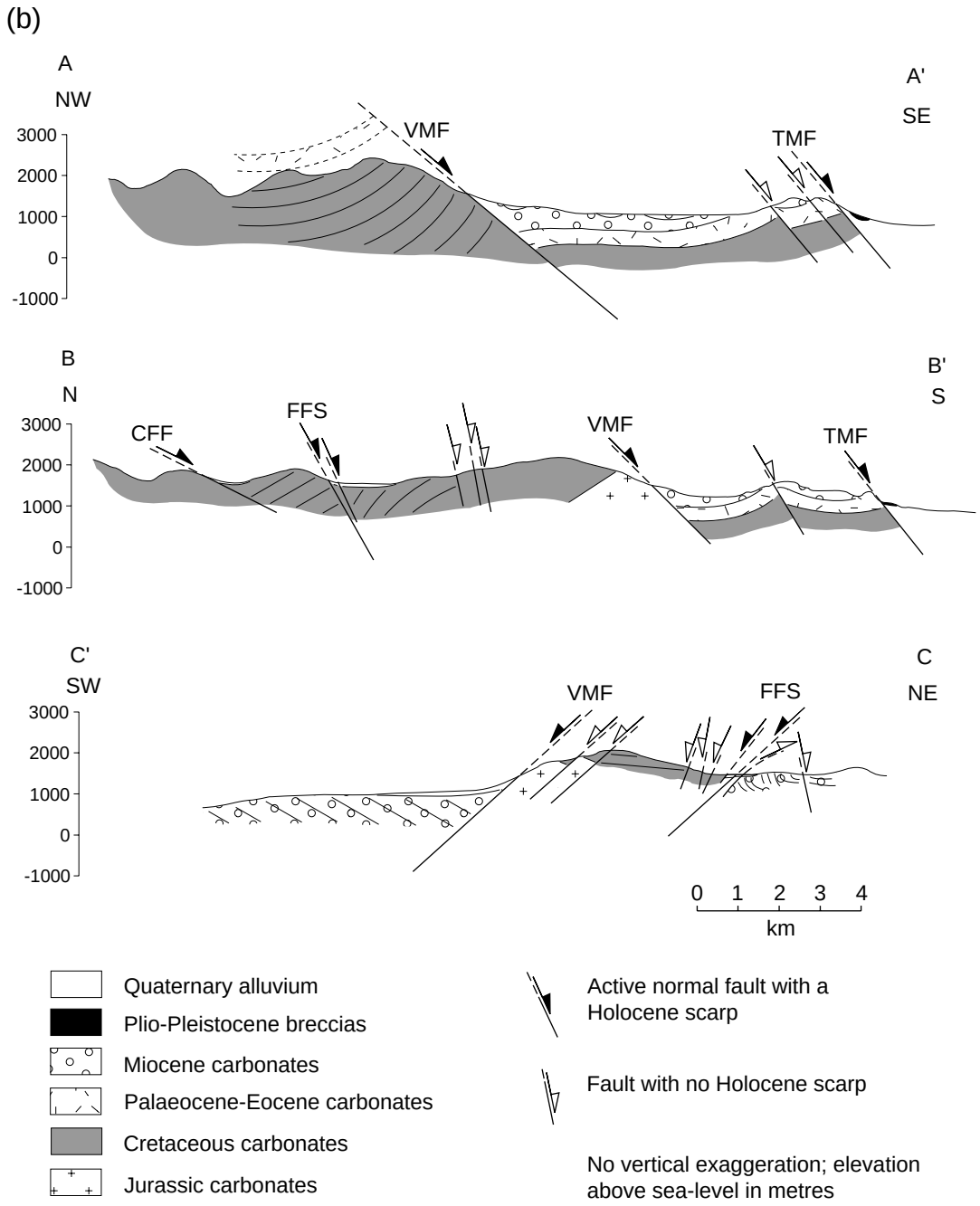

Fig. 5 (*continued*)

FFS over the same time period) (Fig. 3b). Study of propriety seismic data reveals that the VMF accumulated most of its throw during the Pliocene when NE–SW to E–W structures dominated tectonic activity in the area (Galadini and Messina, 1994). These data suggest that the VMF, although a major topography-forming structure (Figs. 1, 2 and 5), may be accommodating approximately N–S extensional strain caused by the slip on the FiFS and FFS. We investigate this further in the following sections.

4.4. The Campofelice fault (CFF)

The NW–SE-trending Campofelice fault outcrops as a Cretaceous limestone scarp for about 5 km and bounds the northeastern edge of Piano di Campofelice (Fig. 7). Recent scree and alluvium are present in the hanging wall. Scarp height reaches a maximum of 4.0 m and decreases to 0.5 m at the NW end. Fault striae indicate almost pure dip-slip movement. Slip directions vary only slightly (198–212°) along the main scarp

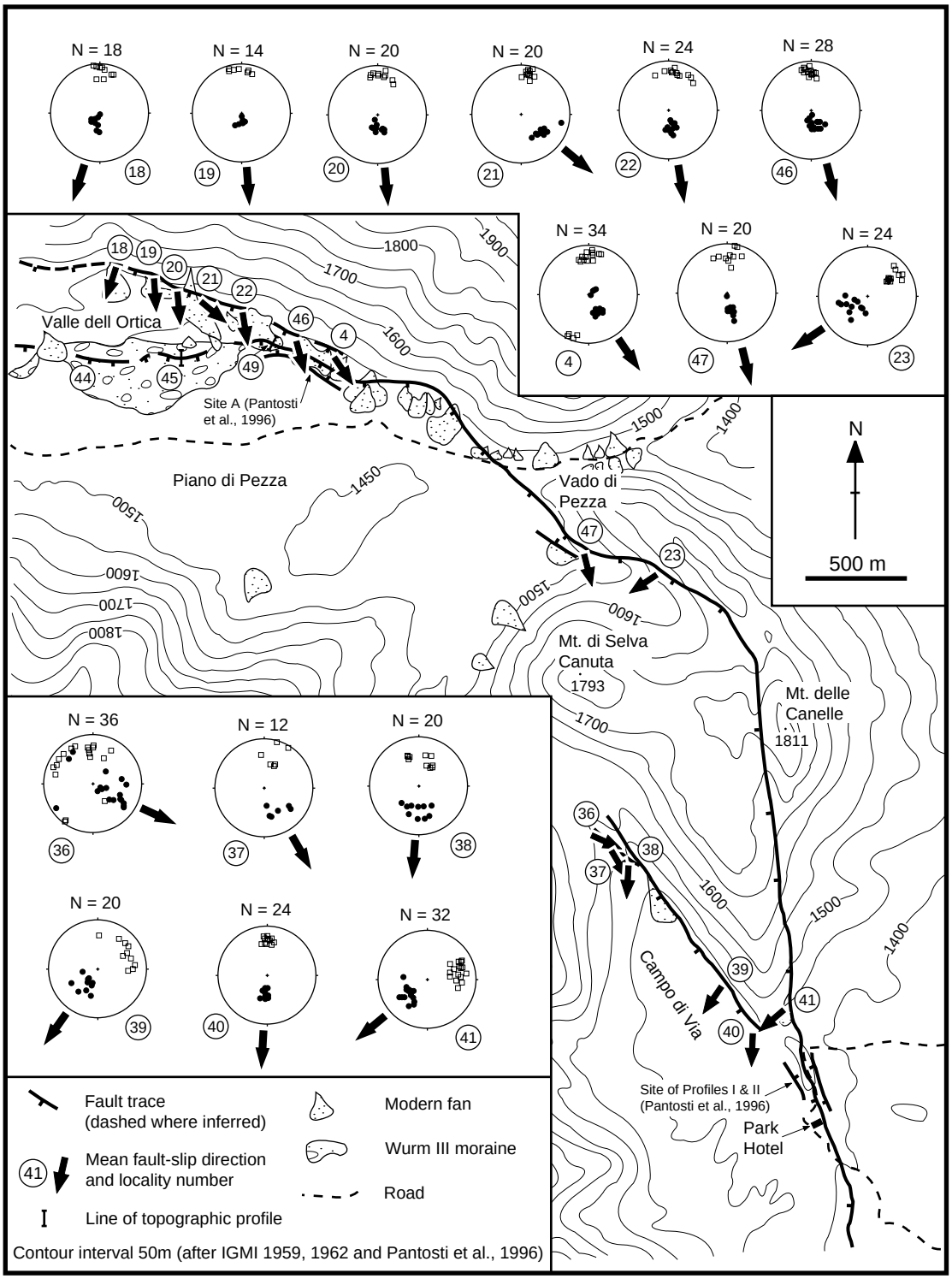

Fig. 6. Map of the northern end of the Fucino fault (FFS) (after Pantosti et al., 1996; their Ovindoli–Pezza fault). The stereonets (lower hemisphere) show poles to fault planes (open squares) and lineations (striations, corrugations) on the fault planes (filled circles). Heavy arrows indicate the mean fault-slip direction for each locality. Locality details are in Table 1.

(Fig. 7; Table 2). The mean slip direction is 206°, nearly 20° different to the regional extension direction of 225°.

The CFF offsets glacial surfaces and so we can use the method described above to estimate minimum deformation rates across the fault. Offset glacial surfaces across the CFF yield rates of throw and displacement of 0.13–0.16 mm/y and 0.17–0.18 mm/y, respectively,

and of horizontal extension of 0.08–0.11 mm/y (Table 2). These rates are far lower than those determined for the FFS and FiFS (see above and Table 1).

4.5. The Tre Monti fault (TMF)

The Tre Monti fault is a NE–SW-trending normal fault which downthrows to the SSE (Fig. 8). The fault outcrops for ~6 km along the southern slopes of Tre Monti as an almost continuous series of Mesozoic limestone scarps, with strikes varying between 035° and 085°. Observed scarp heights vary between 1.0 and 3.0 m. Plio-Pleistocene continental sediments outcrop in the hanging wall and are in places tilted toward the fault scarp (see also Galadini and Messina, 1994). Outcrops in lacustrine and alluvial sediments define a less continuous ENE–WSW fault at the foot of the mountain slope, with upper Pleistocene sediments exposed in its hanging wall but having no clear Holocene scarp [Avezzano–Celano fault (ACF) of Galadini and Messina, 1994]. Fault striae indicate almost pure dip-slip movement along most of the Tre Monti fault. Slip directions vary from 136–200° along the main scarp, with a mean slip direction towards 153° (Fig. 8; Table 2), about 70° different to the regional extension direction.

Offset glacial surfaces were used to estimate minimum deformation rates across the TMF. Rates of throw and displacement are 0.04–0.20 mm/y and 0.04–0.22 mm/y, respectively, and rates of horizontal extension are 0.02–0.09 mm/y (Table 2). These rates are far lower than those determined for the FFS and FiFS (Table 1) and are of similar magnitude to those derived for the VMF and CFF (Table 2).

4.6. Summary

The FiFS and FFS are major NW–SE-trending normal faults that accommodate a portion of the present-day regional NE–SW extension across the central Apennines. Within the en échelon step between the FiFS and FFS, minor normal faults (having lower slip-rates and slip directions generally towards the S rather than the regional SW) such as the VMF and TMF are also active. We interpret the stepover between the FiFS and FFS as a fault segment boundary: the Velino fault segment boundary (VFSB).

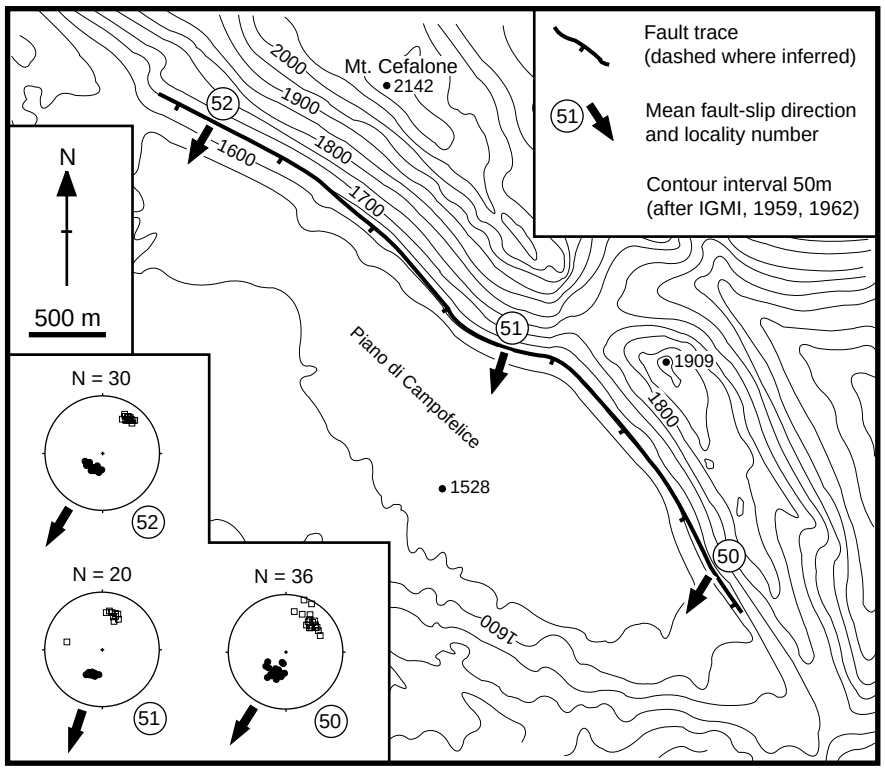

Fig. 7. Map of the Campofelice fault (CFF). The stereonets (lower hemisphere) show poles to fault planes (open squares) and lineations (striations, corrugations) on the fault planes (filled circles). Heavy arrows indicate the mean fault-slip direction for each locality. Locality details are in Table 2.

5. Deformation within the VFSB

The slip directions on the minor faults (CFF, VMF, TMF) change with distance from the centre of the FFS (Figs. 1 and 9). The difference between the mean slip direction and the regional extension direction (at the point of maximum displacement) has been plotted as a function of distance from the centre (point of maximum displacement; point X, Fig. 1b) of the FFS (Fig. 9b). The CFF has a mean slip direction of 206° and is 23 km from the centre of the FFS (line X, Fig. 1b); similarly, the VMF has values of 182° and 15.5 km and the TMF 153° and 9.5 km. A good linear correlation is found (Fig. 9b). The slip directions on these faults appear to be controlled by distance along, and therefore vertical motion across, the FFS.

Rates of horizontal extension across the faults within the VFSB are illustrated with vector arrows in Fig. 9(a). The orientations of the arrows show the directions of movement of the hanging wall relative to

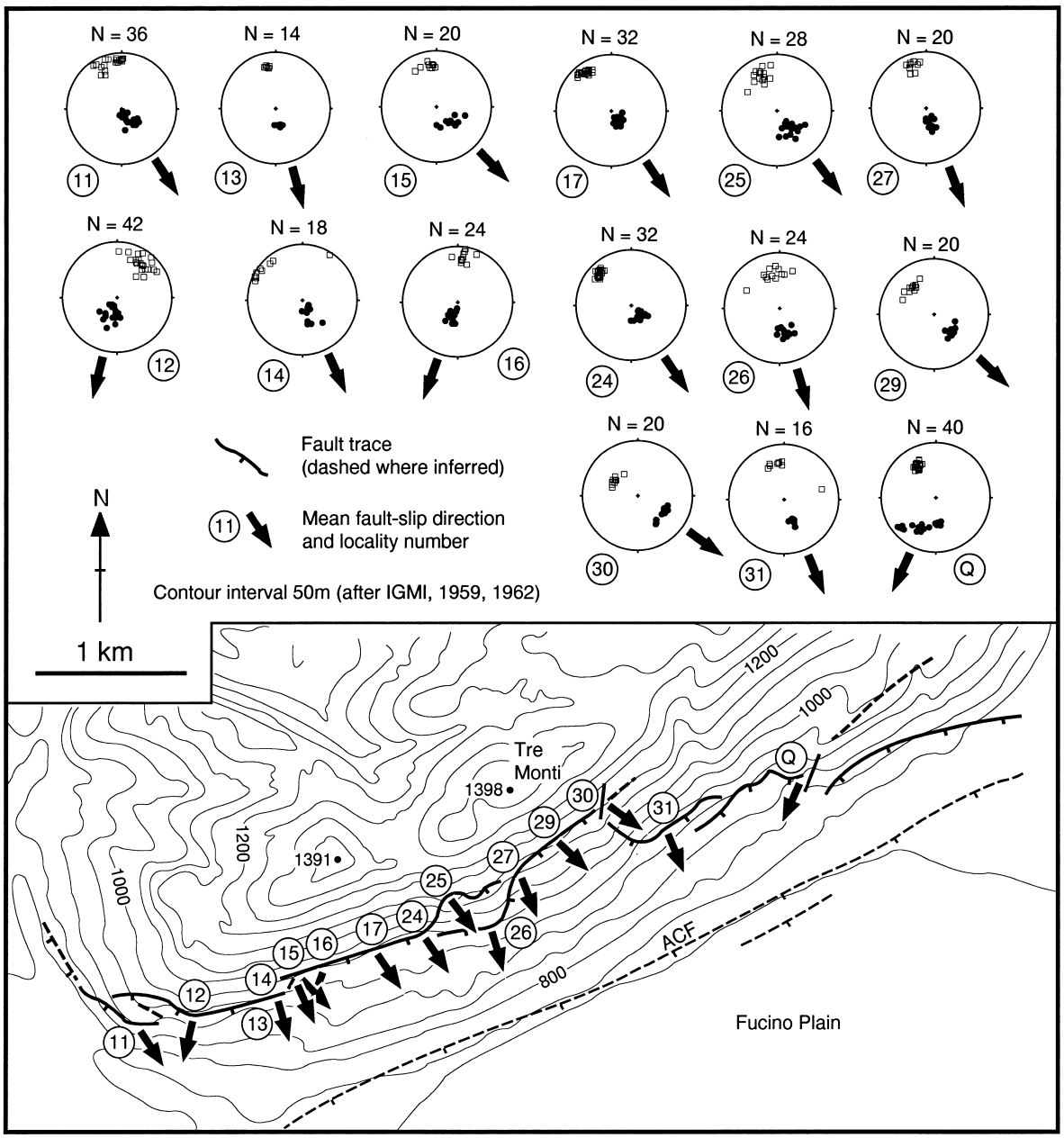

Fig. 8. Map of the Tre Monti fault (TMF) (after Galadini and Messina, 1994). The stereonets (lower hemisphere) show poles to fault planes (open squares) and lineations (striations, corrugations) on the fault planes (filled circles). Heavy arrows indicate the mean fault-slip direction for each locality. Locality details are in Table 2. ACF—Avezzano–Celano fault.

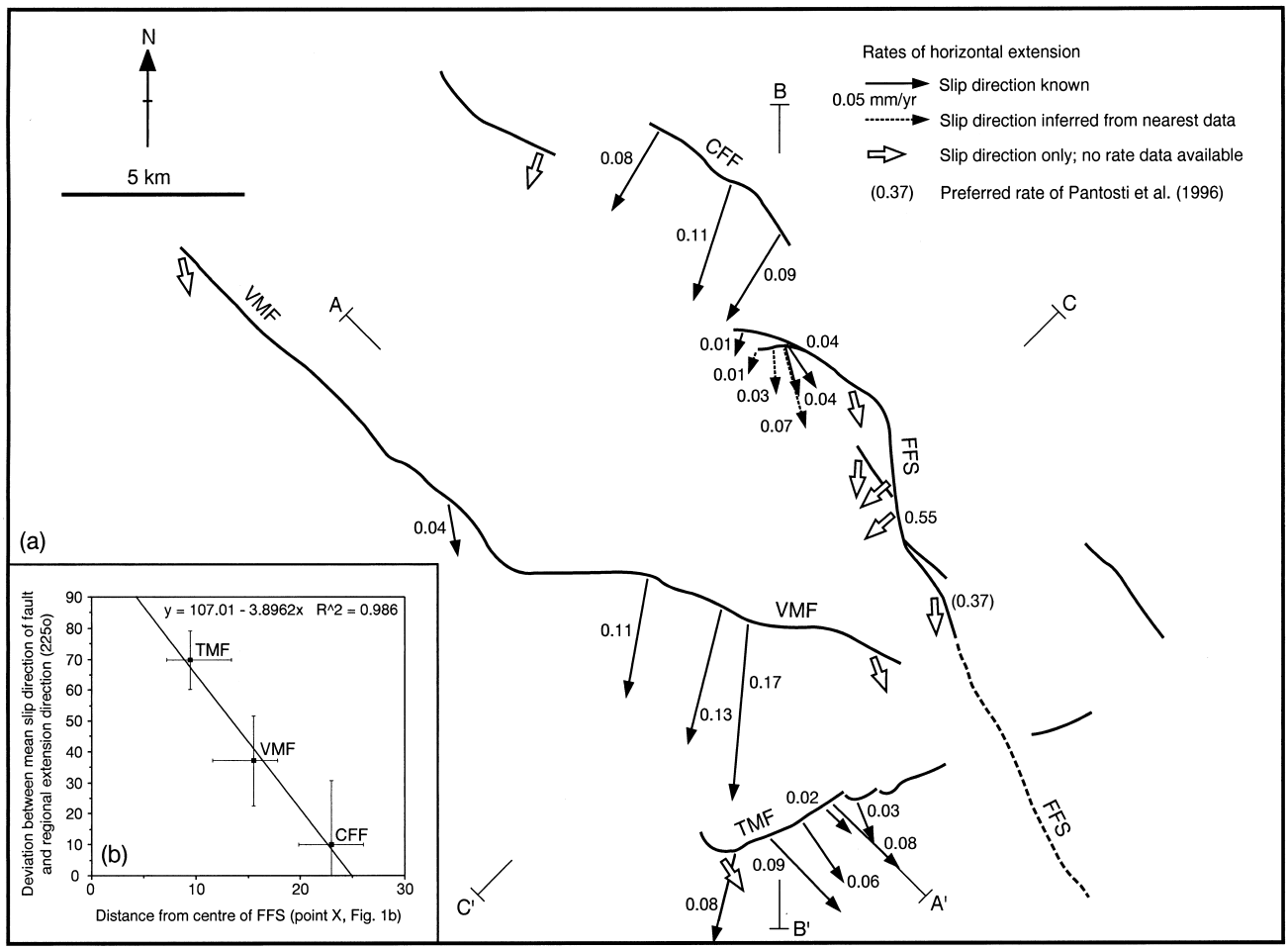

Fig. 9. (a) Horizontal velocity vector arrows for the faults within the Velino fault segment boundary (VFSB), located in Figs. 1(b) and 5(a). Arrows represent the average horizontal extension rate across a fault over the past 18 ka in mm/y in the direction shown and relative to a point in the footwall at each locality. Lines A–A′, etc., indicate transects along which rates have been summed (see text for discussion). (b) Difference between the mean slip direction of a fault and the regional extension direction (225°) plotted as a function of the distance of the fault from the centre of the Fucino fault (FFS) (indicated by 'X' in Fig. 1b). The mean slip direction on a fault tends towards a 90° difference from the regional extension direction as the centre of the FFS is approached. See text for discussion.

points in the immediate footwall and their lengths are proportional to the rates averaged over the past 18 ka. In order to investigate the strain within the VFSB we have summed horizontal extension rates along three transects (Fig. 9a). Transect A–A′ strikes NW–SE, parallel to the FiFS, FFS and the general trend of the Apennine chain; transect B–B′ strikes N–S and intersects all the major faults in the Velino–Magnola area; transect C–C′ strikes NE–SW, parallel to the regional extension across the Apennine chain (Anderson and Jackson, 1987; Ward and Valensise, 1989; Westaway et al., 1989). The nearest calculated rate to the intersection of the transect with a fault was used. Trigonometry was used to calculate the components of motion parallel to the transects where fault-slip is oblique to these directions. The transects are the same length, allowing comparison of their magnitudes. Between them, the transects cover much of the VFSB and therefore provide a representative picture of the strain pattern within the area since 18 ka. The summed extension rate accommodating strike-parallel NW–SE extension along line A–A′ is 0.14 mm/y and accommodating strike-normal NE–SW extension along line C–C′ is 0.68 mm/y. The summed extension rate accommodating N–S extension along line B–B′ is 0.43 mm/y. The three-dimensional strain within the VFSB is predominantly oblate vertical flattening with the x-direction elongated parallel to the regional extension direction (225°) indicated by focal mechanisms and borehole breakout data (Anderson and Jackson, 1987; Ward and Valensise, 1989; Westaway et al., 1989; Amato et al., 1995; Amoruso et al., 1998). This is a similar style of deformation to that described for a segment boundary between two normal faults in the Gulf of Corinth, Greece (Morewood and Roberts, 1997).

It is interesting to note that the NE–SW extension rate across the distributed faults in the VFSB (0.68 mm/y) is similar to that across the centre of the FiFS

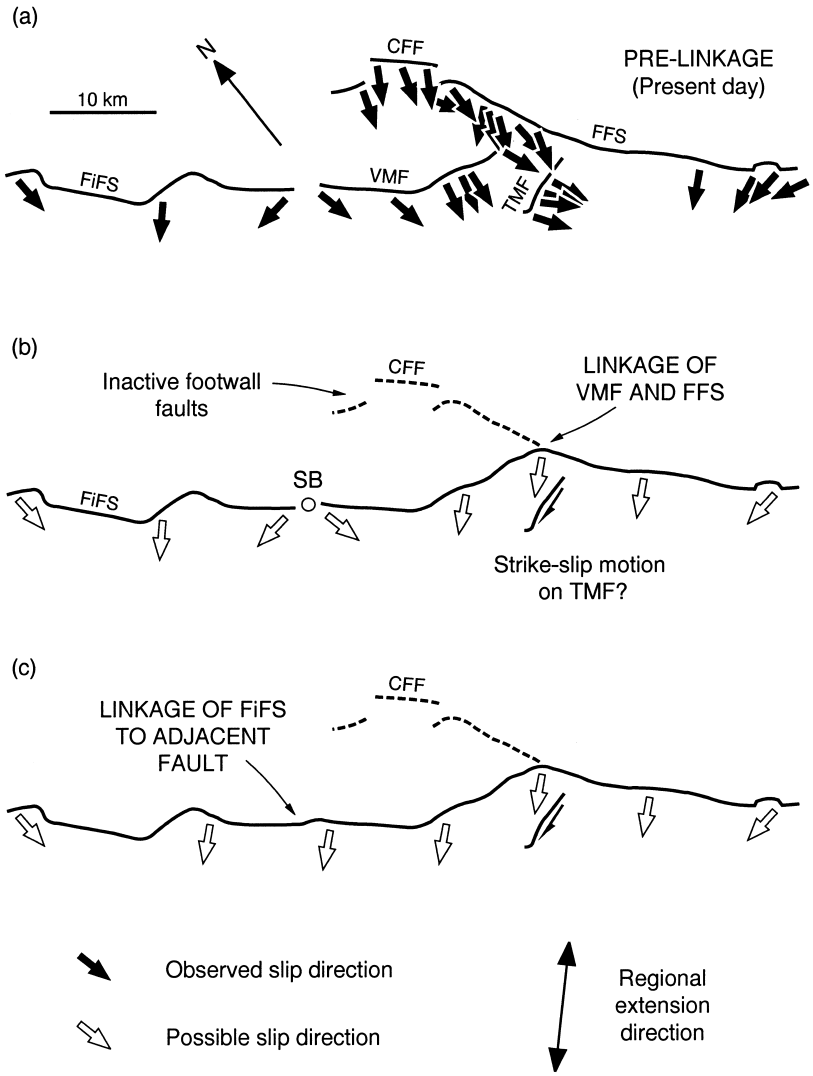

Fig. 10. Possible model for the evolution of the Abruzzo normal fault system. (a) At the present time, slip on the VMF and TMF is controlled by the throw and kinematics on the FFS (see text). (b) Inferred interaction between the VMF and FFS may lead to linkage of the two faults. The northern end of the FFS and the CFF become inactive faults in the footwall of the newly linked fault. The slip direction on the VMF changes to accommodate the regional extension (225°). The TMF, now in the central part of the new fault's hanging wall, may change its kinematics in order to accommodate the change in slip direction on the adjacent part of the new fault. Alternatively, the TMF may become inactive. A segment boundary (SB) may still exist between the new fault and the FiFS (note the difference in slip direction across the segment boundary). (c) Linkage may occur between the FiFS and the larger fault, forming a much longer, single fault. The kinematic pattern on this new fault would be similar to that observed on the FFS and FiFS today, with dip-slip in the central portion, accommodating the regional extension, and oblique-slip towards its ends. See text for discussion.

(0.64 mm/y). Both these values are far less than the NE–SW extension rate across the centre of the FFS (1.60 mm/y). This is interesting because many studies have suggested that segment boundaries are sites of long-term displacement deficit along normal fault systems (e.g. Schwartz and Coppersmith, 1984; Wheeler, 1987, 1989; Crone and Haller, 1989; Zhang et al., 1991). If the NW end of the FFS is ignored in summing the NE–SW extension across the VFSB (perhaps because it bounds rather than forms part of the VFSB) the value would fall to 0.13 mm/y. Alternatively, a longer NE–SW transect that crosses the centres of both the FiFS and the Corno fault (CFS, Fig. 1) gives a summed rate of extension of 0.97 mm/y, a value greater than that for NE–SW extension across the stepover. This may indicate that the FiFS and CFS are acting in unison to maintain the regional extension rate, and that the stepover is an area of slip-deficit. However, some studies have suggested that the summed displacements across segment boundaries or relay zones are comparable to the displacements on the neighbouring faults (Anders and Schlische, 1994; Dawers and Anders, 1995) and our data do not preclude the possibility that there is no deficit in the re-

Table 1
Fault orientation and deformation rate data for the Fiamignano (FiFS) and Fucino (FFS) faults. Disp—displacement; TR—throw rate; DR—displacement rate; HE(R)—horizontal extension (rate). Deformation rates are stated for the vertical plane containing the mean slip-vector azimuth at each locality. Numbers in italics are data inferred from the nearest available data; mean dip and fault-slip direction only. Localities are shown in Figs. 1(b), 5(a) and 6. Sources of trench data are as follows: *1 Galadini et al. (1997); *2 Michetti et al. (1996). Values for localities 41 and 49 are in close agreement with the findings of Pantosti et al. (1996) and are discussed in the text

Locality	Mean strike/dip	Mean slip vector	Total throw (m)	18 ka scarp height (m)	Throw since 18 ka (m)	Disp since 18 ka (m)	HE since 18 ka (m)	TR since 18 ka (mm/y)	DR since 18 ka	HER since 18 ka	
Fiamignano fault segment (FiFS)											
55	138/72	37–262	200	4.0	4.0	6.7	5.3	0.22	0.37	0.29	
56	114/44	41–223	1700	10.0	10.0	15.2	11.5	0.56	0.84	0.64	
7	131/58	44–177	400	4.0	4.0	5.8	4.1	0.22	0.32	0.23	
Fucino fault segment (FFS)											
1	174/66	38/283	300	5.0	5.0	8.1	6.3	0.28	0.45	0.35	
3	117/76	53–176		23.5	23.5	29.4	17.7	1.31	1.63	0.98	
4	086/75	63–146		2.0	1.5	1.7	0.8	0.08	0.09	0.04	
18	096/76	72–198		0.5	0.4	0.4	0.1	0.02	0.02	0.01	
19	093/78	74–176									
20	097/71	66–175									
21	101/75	40–130									
22	103/70	58–171									
23	144/60	58–236									
36	077/73	43–115									
37	108/60	41–150									
38	101/50	47–184									
39	152/66	57–215									
40	091/61	58–183									
41	168/58	48–230		12.0	11.0	14.8	9.9	0.61	0.82	0.55	
44	*70*	*−198*		0.5	0.5	0.5	0.5	0.03	0.03	0.01	
45	*70*	*−176*		2.0	2.0	1.6	0.6	0.10	0.09	0.03	
46	091/68	64–165		2.0	1.5	1.7	0.7	0.08	0.09	0.04	
47	092/68	63–166									
49	*70*	*−165*		5.8	3.6	3.8	1.3	0.20	0.21	0.07	
59	140/73	72–261	600					0.56	0.58	0.20	*1
60	150/54	71–248	800					0.78	0.82	0.28	*1
61	153/46	59–229	1300					1.67	1.94	1.12	*1
62	*70*	*−229*	2200	36.0	36.0	38.3	13.1	2.00	2.13	0.73	
63	112/70	65–197	1400								
64	105/41	42–204	1200	20.0	20.0	29.9	7.3	1.11	1.66	0.41	
65	196/41	50–204	1100	14.5	14.5	18.9	5.3	0.81	1.05	0.29	
66	126/53	44–182	400	11.0	11.0	15.8	4.0	0.61	0.88	0.22	
67	155/44	59–151	400	11.0	11.0	12.8	4.0	0.61	0.71	0.22	
68	153/45	*−229*						1.60	1.60	1.60	*2

gional extension rate across the stepover described here.

6. Discussion

We have shown that three-dimensional strain has developed in the stepover between two major normal faults and is synchronous with plane strain deformation associated with dip-slip faulting at the centres of the major faults. To accommodate this spatial change in the strain, dip-slip at the centres of the major faults becomes progressively more oblique towards their lateral terminations (Fig. 1b). Along-strike extension in the stepover occurs across dip-slip faults oriented obliquely to the major faults (e.g. VMF and TMF). This is similar to the release fault geometry described by Destro (1996). The slip directions on the faults within the stepover become more oblique to the regional extension direction as the centre of the FFS is approached. Slip directions on these small dip-slip faults appear to be controlled by distance, and therefore throw variation, along the major fault (the FFS). This relationship between the throw and kinematics of the major fault and the minor hanging wall faults is interesting and, to our knowledge, has not been previously reported.

Along-strike extension in the stepover is probably mainly due to subsidence of the neighbouring FFS hanging wall basin and associated stretching of the

Table 2
Fault orientation and deformation rate data for the Velino–Magnola (VMF), Tre Monti (TMF) and Campofelice (CFF) faults. Localities are shown in Fig. 5(a), 7 and 8. Details as for Table 1

Locality	Mean strike/dip	Mean slip vector	18 ka scarp height (m)	Throw since 18 ka (m)	Disp since 18 ka (m)	HE since 18 ka (m)	TR since 18 ka (mm/y)	DR since 18 ka	HER since 18 ka
Velino–Magnola fault (VMF)									
5	094/76	62–159							
6	083/49	46–185	4.8	3.5	4.6	3.0	0.19	0.26	0.17
32	124/58	56–194	5.0	3.4	4.1	2.3	0.19	0.23	0.13
33	083/73	71–167							
34	089/63	58–170	2.0	1.4	1.6	0.7	0.08	0.09	0.04
35	117/60	52–193	5.0	3.4	3.9	2.0	0.19	0.22	0.11
Tre Mont1 fault (TMF)									
11	073/76	71–147							
12	127/68	64–194	8.0	3.6	3.9	1.5	0.2	0.22	0.08
13	079/65	63–165							
14	043/85	63–156							
15	080/65	57–136	3.2	2.4	2.9	1.6	0.13	0.16	0.09
16	097/72	66–200							
17	058/72	71–146							
24	046/71	68–146	3.0	2.4	2.6	1.0	0.13	0.14	0.06
25	064/60	52–143							
26	080/56	61–164							
27	072/69	67–159							
28	065	*−134*	1.0	0.7	0.8	0.3	0.04	0.04	0.02
29	048/55	52–134	2.5	1.8	2.3	1.4	0.1	0.13	0.08
30	033/42	41–126							
31	082/60	53–158	1.0	0.7	0.9	0.5	0.04	0.05	0.03
Campofelice fault (CFF)									
50	132/63	59–212	4.0	2.8	3.3	1.7	0.16	0.18	0.09
51	107/56	52–198	4.0	2.4	3.1	1.9	0.13	0.17	0.11
52	129/66	64–211	4.0	2.9	3.2	1.4	0.16	0.18	0.08

hanging wall surface; the VMF and TMF downthrow towards this basin (Fig. 1). Similar mechanisms for along-strike extension at the ends of normal faults have been suggested by Anders et al. (1990) for the northeastern Basin and Range, USA, and by Morewood and Roberts (1997) for the eastern Gulf of Corinth, Greece. Subsidence of the FiFS hanging wall basin appears to have little effect on the kinematics within the stepover, perhaps because of the left-stepping geometry of the fault system.

Earlier we stated that knowledge of the geometry, kinematics and rates of extension in stepover zones prior to fault linkage might help us understand how deformation proceeds during linkage across such zones. In the pre-linkage example described in this paper, distributed along-strike extension in the stepover (0.14 mm/y) has proceeded at a rate of 13–22% of that for fault-normal extension at the centres of the major faults (1.12 mm/y, FFS; 0.64 mm/y, FiFS) over at least the past 18 ka. Although not directly analogous, these values are similar to rates of along-strike motion at the lateral terminations of isolated normal faulting earthquake ruptures compared to those for slip at the centre of the rupture, both for elastic half-space models (20%) (Ma and Kusznir, 1995) and for a natural example measured geodetically using GPS following the 1995 Kozani–Grevena earthquake ($M_s \simeq 6.6$), Greece (8–14%) (Clarke et al., 1997). Similar characteristics were also observed for a segment boundary in the Gulf of Corinth, Greece (Morewood and Roberts, 1997). The actual values for along-strike extension within the stepover presumably scale with the slip-rates on the bounding major faults. The point here is that along-strike extension in stepovers is significant when compared to fault-normal slip across the centres of the major faults. However, following linkage, individual locations in the stepover would either be part of the hanging wall or footwall of the new, longer, linked fault, and would themselves be subsiding or uplifting (Fig. 10). Presumably, following linkage, along-strike extension would cease in the area previously occupied by the stepover and be replaced by plane strain deformation similar to that at the centres of the pre-linkage major faults (Fig. 10). Dip-slip faults oriented obliquely to the major faults within former stepovers would presumably either (1) become inactive

following linkage, due to the cessation of along-strike extension, or (2) change their kinematics to accommodate a slip direction parallel to the regional extension direction (e.g. TMF, Fig. 10). Thus, the geometry, kinematics and rates of deformation within the stepover would change in some way at the time of linkage. Our linkage model (Fig. 10) is only a possible evolution for the studied fault system based on the observed data and other models for the growth of fault systems (e.g. Cartwright et al., 1995, 1996; Cowie, 1998). The point is that we do not know how the kinematics of fault systems evolve through time. Detailed studies of mature fault systems may enhance our knowledge regarding this subject.

The above implies that the rates of fault-slip for release faults in stepovers are not controlled simply by the regional extension rate and the number of active faults of given dimensions in the fault system (cf. Nicol et al., 1997). Rather, their slip-rates are controlled by a combination of (1) the above, (2) the rates of slip of the neighbouring major faults and (3) the stage in the linkage process that has been achieved. The above underlines the conclusion that slip rates can be controlled by fault interaction and the stage in the linkage-growth history achieved by the faults (e.g. Cowie, 1998). However, here we show that the slip rates and kinematics, and hence the strain patterns along fault systems can only be understood when the location of the area to be considered is known in relation to the positions of present and past stepovers.

7. Conclusions

1. The FiFS and FFS are major NW–SE-trending faults that accommodate a proportion of the present-day regional NE–SW extension across the central Apennines.
2. Within the en échelon step between the FiFS and FFS, minor faults (having lower slip-rates and slip directions towards the S rather than the regional SW) such as the VMF and TMF are also active. We interpret the stepover between the FiFS and FFS as a segment boundary: the Velino fault segment boundary (VFSB).
3. Slip-vector azimuths defined by striations on the faults within the VFSB indicate NE–SW extension on NW–SE faults, sub-parallel to the regional extension direction, together with significant and contemporaneous (during the last 18 ka) NW–SE extension on ESE–WNW and ENE–WSW faults.
4. Three-dimensional strain occurs within the VFSB, as opposed to the plane strain across the centres of the major bounding faults (FiFS and FFS). Similar strain distributions have been described elsewhere and may be common within actively extending areas worldwide.
5. High fault-normal extension, relative to one of the neighbouring faults (FiFS), is observed across the stepover (VFSB).
6. Slip directions on release faults in the hanging walls of major faults become more oblique to the regional extension direction as the centre of a major fault is approached.
7. Slip directions for faults in stepovers are controlled by both the regional extension and local subsidence/uplift variations along the major bounding faults.
8. Slip-rates for release faults in stepovers are controlled by (i) the regional extension rate, (ii) the number of active faults of given dimension in the fault system, (iii) the rates of slip of the neighbouring major faults and (iv) the stage in the linkage process that has been achieved.

Acknowledgements

This study was funded by a Birkbeck College Research Scholarship (NCM) and NERC GR9/02995 and Birkbeck College (GPR). The Benfield Greig Hazard Research Centre at UCL is thanked for support. Caroline Coyle is thanked for assistance during fieldwork. This work benfited from discussions with Alessandro Michetti. Mark Anders and Nancye Dawers provided thorough and helpful reviews of the original manuscript.

References

Amato, A., Montone, P., Cesaro, M., 1995. State of stress in Southern Italy from borehole breakout and focal mechanism data. Geophysical Research Letters 22, 3119–3122.

Amoruso, A., Crescentini, L, Scarpa, R., 1998. Inversion of source parameters from near- and far-field observations: An application to the 1915 Fucino earthquake, central Apennines, Italy. Journal of Geophysical Research 103, 29,989–29,999.

Anders, M.H., Schlische, R.W., 1994. Overlapping faults, intrabasin highs, and the growth of normal faults. Journal of Geology 102, 165–180.

Anders, M.H., Geissman, J.W., Sleep, N.H., 1990. Comment on 'Northeastern Basin and Range province active tectonics: An alternative view'. Geology 18, 914–917.

Anderson, H., Jackson, J., 1987. Active tectonics of the Adriatic Region. Geophysical Journal of the Royal Astronomical Society 91, 937–983.

Biasini, A., 1966. Elementi morfotettonici, tratti da un rilievo fotogeologico al margine dell'altipiano di Ovindoli. Geol. Rom. 5, 303–312.

Blumetti, A.M., Michetti, A.M., Serva, L., 1987. The ground effects of the Fucino earthquake of Jan. 13th, 1915; an attempt for the understanding of the recent geological evolution of some tectonic structures. In: Margottini, C., Serva, L. (Eds.), Historical seismi-

city of central-eastern Mediterranean region. Proceedings of the 1987 ENEA–IAEA International Workshop, pp. 297–320.

Cartwright, J.A., Trudgill, B.D., Mansfield, C.S., 1995. Fault growth by segment linkage: an explanation for scatter in maximum displacement and trace length data from the Canyonlands Grabens of SE Utah. Journal of Structural Geology 17, 1319–1326.

Cartwright, J.A., Mansfield, C., Trudgill, B., 1996. The growth of normal faults by segment linkage. In: Buchanan, P.G., Nieuwland, D.A. (Eds.), Modern Developments in Structural Interpretation, Validation and Modelling, Geological Society Special Publication, 99, pp. 163–177.

Cinti, F.R., D'Addezio, G., Pantosti, D., Hamilton, J., 1992. Ricostruzione topographica di dettaglio della scarpata di faglia del Piano di Pezza, Abruzzo. Studi Geol. Camerti 1992/1, 115–122.

Clarke, P.J., Paradissis, D., Briole, P., England, P.C., Parsons, B.E., Billiris, H., Veis, G., Ruegg, J.-C., 1997. Geodetic investigation of the 13 May 1995 Kozani–Grevena (Greece) earthquake. Geophysical Research Letters 24, 707–710.

C.N.R. (Consiglio Nazionale delle Ricerche), 1983. Structural Model of Italy, Sheet No. 4. Progetto Finalizzato Geodynamica, Modello Strutturale Tridimensionale, scale 1:500,000.

Cowie, P.A., 1998. A healing–reloading feedback control on the growth rate of seismogenic faults. Journal of Structural Geology 20, 1075–1087.

Crone, A.J., Haller, K.M., 1989. Segmentation of Basin and Range normal faults: examples from east-central Idaho and southwestern Montana. In: Schwartz, D.P., Sibson, R.H. (Eds.), Proceedings of Conference XLV, Directions in Palaeoseismology, U.S. Geological Survey Open-File Report, 89–315, pp. 110–130.

Dawers, N.H., Anders, M.H., 1995. Displacement–length scaling and fault linkage. Journal of Structural Geology 17, 607–614.

Destro, N., 1996. Release fault: A variety of cross fault in linked extensional fault systems, in the Sergipe–Alagoas Basin, NE Brazil. Journal of Structural Geology 17, 615–629.

Galadini, F., Messina, P., 1994. Plio-Quaternary tectonics of the Fucino basin and surrounding areas (central Italy). Giornale di Geologia 56, 73–99.

Galadini, F., Galli, P., Giraudi, C., 1997. Geological investigations of Italian earthquakes: new paleoseismological data from the Fucino plain (central Italy). Journal of Geodynamics 24, 87–103.

Giraudi, C., 1989. Datazione con metodi geologici delle scarpate di faglia post-glaciali di Ovindoli–Piano di Pezza (Abruzzo—Italia centrale): Implicazoni. Memorie della Societa Geologica Italiana 42, 29–39.

Giraudi, C., 1992. Segnalazione di scarpate di faglia tardo-pleistoceniche sui Monti della Magnola (Massiccio del Velino–Abruzzo). Il Quaternario 5, 27–32.

Giraudi, C., 1995. Considerations on the significance of some post-glacial fault scarps in the Abruzzo Apennines (central Italy). Quaternary International 25, 33–45.

Giraudi, C., Frezzotti, M., 1997. Late Pleistocene glacial events in the Central Apennines, Italy. Quaternary Research 48, 280–290.

I.G.M.I. (Instituto Geografico Militare Italia), 1959. Topographic Map of Italy, Avezzano sheet. Serie M691, Foglio 145, scale 1:100,000.

I.G.M.I. (Instituto Geografico Militare Italia), 1962. Topographic Map of Italy, Sulmona sheet. Serie M691, Foglio 146, scale 1:100,000.

Ma, X.Q., Kusznir, N.J., 1995. Coseismic and postseismic subsurface displacements and strains for a dip-slip normal fault in a three-layer elastic-gravitational medium. Journal of Geophysical Research 100, 12,813–12,828.

Margottini, C., Screpanti, A., 1988. Temporal evolution of the seismic crisis related to the 13th January 1915, Avezzano earthquake. In: Margottini, C., Serva, L. (Eds.), Historical seismicity of central-eastern Mediterranean region. Proceedings of the 1987 ENEA–IAEA International Workshop, pp. 185–193.

Michetti, A.M., Brunamonte, F., Serva, L., Vittori, E., 1996. Trench investigations of the 1915 Fucino earthquake fault (Abruzzo, central Italy): Geological evidence of large historical events. Journal of Geophysical Research 101, 5921–5936.

Michetti, A.M., Ferreli, L., Vittori, E., Serva, L., Blumetti, A.M., Esposito, E., Porfido, S., Roberts, G.P., 2000. Ground effects during the September 9, 1998, $M_w = 5.6$, Lauria earthquake: seismic potential of the aseismic Pollino region in Southern Italy. Seismological Research Letters, in press.

Morewood, N.C., Roberts, G.P., 1997. Geometry, kinematics and rates of deformation in a normal fault segment boundary, central Greece. Geophysical Research Letters 24, 3081–3084.

Nicol, A., Walsh, J.J., Watterson, J., Underhill, J.R., 1997. Displacement rates of normal faults. Nature 390, 157–159.

Nijman, W., 1971. Tectonics of the Velino–Sirente area, Abruzzi, central Italy. Koninkl. Nederl. Akademie van Wetenschappen, Series B 74 (2), 156–184.

Oddone, E., 1915. Gli elementi fisici del grande terremoto marsicano fucense del 13 Gennaio 1915. Bollettino della Societa Sismologica Italiana 19, 71–215.

Pantosti, D., D'Addezio, G., Cinti, F.R., 1996. Paleoseismicity of the Ovindoli–Pezza fault, central Apennines, Italy: A history including a large, previously unrecorded earthquake in the Middle Ages (860–1300 A.D.). Journal of Geophysical Research 101, 5937–5959.

Patacca, E., Sartori, R., Scandone, P., 1990. Tyrrhenian Basin and Apenninic Arcs: Kinematic relations since late Tortonian times. Memorie della Societa Geologica Italiana 45, 425–451.

Peacock, D.C.P., Sanderson, D.J., 1991. Displacements, segment linkage and relay ramps in normal fault zones. Journal of Structural Geology 13, 721–733.

Peacock, D.C.P., Sanderson, D.J., 1994. Geometry and development of relay ramps in normal fault systems. American Association of Petroleum Geologists Bulletin 78, 147–165.

Roberts, G.P., 1996. Variation in fault-slip directions along active and segmented normal fault systems. Journal of Structural Geology 18, 835–845.

Roberts, G.P., Ganas, A., 2000. Fault-slip directions in central-southern Greece measured from striated and corrugated fault planes: comparison with focal mechanism and geodetic data. Journal of Geophysical Research, in press.

Schwartz, D.P., Coppersmith, K.J., 1984. Fault behaviour and characteristic earthquakes—examples from the Wasatch and San Andreas fault zones. Journal of Geophysical Research 89, 5681–5698.

Serva, L., Blumetti, A.M., Michetti, A.M., 1988. Gli effeti sul terreno del terremoto del Fucino (13.01.1915); tentativo di interpretazione della evoluzione tettonica recente di alcune strutture. Memorie della Societa Geologica Italiana 35, 893–907.

Trudgill, B., Cartwright, J., 1994. Relay-ramp forms and normal-fault linkages, Canyonlands National Park, Utah. Geological Society of America Bulletin 106, 1143–1157.

Ward, S.N., Valensise, G., 1989. Fault parameters and slip distribution of the 1915 Avezzano, Italy, earthquake derived from geodetic observations. Bulletin of the Seismological Society of America 79, 690–710.

Westaway, R., Gawthorpe, R., Tozzi, M., 1989. Seismological and field observations of the 1984 Lazio–Abruzzo earthquakes: implications for the active tectonics of Italy. Geophysical Journal of the Royal Astronomical Society 98, 489–514.

Wheeler, R.L., 1987. Boundaries between segments of normal faults—criteria for recognition and interpretation. In: Crone, A.J., Omdahl, E.M. (Eds.), Proceedings of Conference XXXIX, Directions in Palaeoseisomology, U.S. Geological Survey Open-File Report, 87–673, pp. 385–398.

Wheeler, R.L., 1989. Persistent segment boundaries on Basin–Range normal faults. In: Schwartz, D.P., Sibson, R.H. (Eds.), Proceedings of Conference XLV, Fault segmentation and controls of rupture initiation and termination, U.S. Geological Survey Open-File Report, 89–315, pp. 432–444.

Zhang, P., Slemmons, D.B., Mao, F., 1991. Geometric pattern, rupture termination and fault segmentation of the Dixie Valley–Pleasant Valley active normal fault system, Nevada, U.S.A. Journal of Structural Geology 13, 165–176.